Journal of Mathematical Physics ARTICLE scitation.org/journal/jmp

The closeness of localized structures between the Ablowitz–Ladik lattice and discrete nonlinear Schrödinger equations: Generalized AL and DNLS systems

Cite as: J. Math. Phys. 63, 042701 (2022); doi: 10.1063/5.0072391
Submitted: 22 September 2021 • Accepted: 30 March 2022 •
Published Online: 19 April 2022

Dirk Hennig,[1] Nikos I. Karachalios,[1,a)] and Jesús Cuevas-Maraver[2,3]

AFFILIATIONS

[1] Department of Mathematics, University of Thessaly, Lamia GR 35100, Greece
[2] Grupo de Física No Lineal, Departamento de Física Aplicada I, Universidad de Sevilla, Escuela Politécnica Superior, C/ Virgen de África, 7, 41011 Sevilla, Spain
[3] Instituto de Matemáticas de la Universidad de Sevilla (IMUS), Edificio Celestino Mutis, Avda. Reina Mercedes s/n, 41012 Sevilla, Spain

[a)] **Author to whom correspondence should be addressed:** karan@uth.gr

ABSTRACT

The Ablowitz–Ladik system, being one of the few integrable nonlinear lattices, admits a wide class of analytical solutions, ranging from exact spatially localized solitons to rational solutions in the form of the spatiotemporally localized discrete Peregrine soliton. Proving a closeness result between the solutions of the Ablowitz–Ladik system and a wide class of Discrete Nonlinear Schrödinger systems in a sense of a continuous dependence on their initial data, we establish that such small amplitude waveforms may be supported in nonintegrable lattices for significantly large times. Nonintegrable systems exhibiting such behavior include a generalization of the Ablowitz–Ladik system with power-law nonlinearity and the discrete nonlinear Schrödinger equation with power-law and saturable nonlinearities. The outcome of numerical simulations illustrates, in excellent agreement with the analytical results, the persistence of small amplitude Ablowitz–Ladik analytical solutions in all the nonintegrable systems considered in this work, with the most striking example being that of the Peregine soliton.

I. INTRODUCTION

The Ablowitz–Ladik (AL) equation,[1–3]

$$i\dot{\psi}_n = \kappa\nu(\psi_{n+1} - 2\psi_n + \psi_{n-1}) + \mu|\psi_n|^2(\psi_{n+1} + \psi_{n-1}), \quad n \in \mathbb{Z}, \tag{1.1}$$

is the famous integrable discretization of the cubic nonlinear Schrödinger partial differential equation (PDE),

$$i\partial_t u + \nu u_{xx} + \gamma|u|^2 u = 0, \quad x \in \mathbb{R}. \tag{1.2}$$

The integrability of (1.1) was proved by the discrete version of the inverse scattering transform.[1] The AL is one of the few known completely integrable (infinite) lattice systems admitting exact soliton solutions.[4–7] The one-soliton solution of AL reads[1,2] as follows:

$$\begin{aligned} \psi_n^s &= \frac{\sinh\beta}{\sqrt{\mu}}\operatorname{sech}[\beta(n-ut)]\exp(-i(\omega t-\alpha n)),\\ \omega &= -2\cos\alpha\cosh\beta,\\ u &= 2\beta^{-1}\sin\alpha\sinh\beta, \end{aligned} \tag{1.3}$$

with $\alpha\in[-\pi,\pi]$ and $\beta\in[0,\infty)$. In Refs. 8 and 9, it was shown that the AL equation (1.1) admits [again in similarity with the integrable Nonlinear Schrödinger (NLS) equation (1.2)] rational solutions as the discrete counterpart of the Peregrine soliton (AL-PS),

$$\psi_n^r(t) = q\left[1-\frac{4(1+q^2)(1+4iq^2t)}{1+4n^2q^2+16q^4t^2(1+q^2)}\right]e^{2iq^2t}, \tag{1.4}$$

where the parameter q fixes a background amplitude. Such exact solutions do not exist for the the more relevant (with regard to applications in physics) non-integrable Discrete Nonlinear Schrödinger (DNLS) equation,

$$i\dot{\phi}_n+\kappa\nu(\phi_{n+1}-2\phi_n+\phi_{n-1})+\gamma|\phi_n|^2\phi_n=0,\quad n\in\mathbb{Z},\quad \gamma\in\mathbb{R}. \tag{1.5}$$

However, in Ref. 10, we established the closeness of the solutions of the AL system (1.1) to the DNLS (1.5) in the l^2 and l^∞-metrics in a sense of a continuous dependence on their initial data. The most significant application of this closeness result is that the DNLS lattice admits small amplitude solutions of the order $\mathcal{O}(\varepsilon)$ that stay $\mathcal{O}(\varepsilon^3)$-close to the analytical solutions of the AL for any finite time $0<T_f<\infty$. Furthermore, taking the advantages offered by the discrete ambient space, we extended the result to higher dimensional lattices and other examples of nonlinearities. The numerical studies of Ref. 10, for the persistence of the AL-soliton in the cubic DNLS (1.5) and the saturable one (see below), corroborated to high accuracy the analytical predictions, that these non-integrable DNLS models sustain small amplitude solitary waves preserving for significantly large time intervals, the functional form and characteristics (as the velocity) of the analytical AL-one-soliton solution.

In the present paper, we provide further analytical and numerical extensions of the results of Ref. 10: On the analytical side, we establish the closeness of the solutions between the generalization of the Ablowitz–Ladik (G-AL) lattice,

$$i\dot{U}_n=\kappa\nu(U_{n+1}-2U_n+U_{n-1})+\delta|U_n|^{2\sigma}(U_{n+1}+U_{n-1}),\quad n\in\mathbb{Z}, \tag{1.6}$$

and the integrable AL (1.1). Our study in this paper for the G-AL (1.6) is motivated by the work in Ref. 11, where numerous features were explored, ranging from the derivation of conservation laws of the model, the numerical identification of discrete solitons, and the study of their stability—as the nonlinearity exponent σ is varied—through extended Vakhitov–Kolokolov criteria, to the presentation of numerical evidence for quasi-collapse as indicated by the appearance of large amplitudes for large values of σ. The results of Ref. 11 justified that the G-AL (1.6) similar to the other important generalized DNLS models with power nonlinearity,[12–14]

$$F(z)z=\gamma|z|^{2\sigma}z, \tag{1.7}$$

is significant for the study of the transition from integrability when $\sigma=1$ to non-integrability for $\sigma>1$, and the potential structural changes to the dynamics of intrinsic localized modes possessed by these systems.[13,15] In this regard, we think that our closeness approach is of particular relevance: it simultaneously establishes the existence and persistence of small amplitude localized waveforms for a general class of non-integrable DNLS systems, which approximate the functional form of the analytical solutions of the integrable AL (1.1). As mentioned above, the analysis also covers the DNLS with saturable nonlinearity,

$$F(z)z=\frac{\gamma z}{1+|z|^2}, \tag{1.8}$$

a model governing the dynamics of photo-refractive media; we refer to the works[16–20] concerning the propagation and stability of discrete solitons. Thus, extra motivation is given to pursue further numerical studies exploring the closeness of solutions of the integrable AL to the solutions of the above generalized G-AL and DNLS systems.

The presentation of this paper is as follows: in Sec. II, we recall useful information on the conserved quantities and the Hamiltonian structure of the AL and DNLS lattices studied herein. In Sec. III, we prove the closeness of the solutions between the integrable AL (1.1) and its generalization (1.6). The proof follows the lines in Ref. 10, aided this time, by the nontrivial conserved quantity of the G-AL, which involves the Gauss hypergeometric function.[11] We also prove that the solutions remain close in the sense of momenta. Section IV is devoted to the numerical studies and is divided into three parts. In Subsection IV A, we present the results of the numerical study concerning the persistence of small amplitude single-soliton solutions (1.3) of the AL in the quartic G-AL (1.6), corresponding to the case $\sigma=2$. It is shown that the AL-soliton persists when implemented as an initial condition to the G-AL for significantly large times. Furthermore, the numerical results for

the evolution of the norms of the distance function of the corresponding solutions not only fulfill but also turn out to be even sharper than the respective analytical estimates. A notable feature is that the evolving soliton in the G-AL lattice preserves with a high accuracy the speed of the analytical AL-soliton solution, as well as, its momentum. The same excellent agreement with the analytical predictions is illustrated in Subsection IV B for the dynamics of the analytical AL-soliton in the DNLS with the power nonlinearity (1.7) in its quintic case $\sigma = 2$. We also test the limits of the analytical persistence results regarding the smallness of the amplitudes of the AL-soliton initial conditions in the cubic $\sigma = 1$ and in the quintic DNLS $\sigma = 2$. While the analytical estimates are again satisfied, we find that the persistence of the AL-soliton in these non-integrable lattices lasts for significantly lower times (in comparison to the smaller amplitude cases); this is in accordance with the analysis, as our closeness results rely, in the notion of continuous dependence, on the initial conditions. Furthermore, we observe the emergence of novel dynamical features: in the cubic DNLS, the AL-soliton evolves as a high time-period-spatially localized breather, while in the quintic DNLS, we observe a self-similar decay of the initial condition. Still, in both cases, we observe the preservation of the speed of the initial pulse. Subsection IV D concludes with the presentation of a particularly interesting application of the closeness of the solution approach: the persistence of small amplitude rational solutions of the form of the AL-PS (1.4). Remarkably, and yet in excellent agreement with the analytical considerations, the numerical findings corroborate the existence/persistence of spatiotemporal localized waveforms significantly close to the AL-PS, in all the cases of the non-integrable lattices considered herein. Finally, Sec. V summarizes the main findings and gives an outlook to extensions for future studies.

II. CONSERVED QUANTITIES AND SYMPLECTIC STRUCTURE OF THE AL AND DNLS SYSTEMS

For simplicity, we set in (1.1), (1.5), and (1.6), $\kappa = \nu = 1$. It is useful to recall that all the lattice systems, which are subject of the present study, are particular cases of the general lattice dynamical system studied in Refs. 11, 23, and 24,

$$i\dot{A}_n + f(|A_n|^2)(A_{n+1} + A_{n-1}) + F(|A_n|^2)A_n = 0. \tag{2.1}$$

Considering the functions

$$g(\rho) = \int_0^\rho \frac{dy}{f(y)}, \quad G(\rho) = \int_0^\rho \frac{F(y)dy}{f(y)},$$

it can be proved that the system admits a Hamiltonian structure with the Hamiltonian

$$H = \sum_{n\in\mathbb{Z}} \overline{A}_n(A_{n+1} + A_{n-1}) + \sum_{n\in\mathbb{N}} G(|A_n|^2).$$

Then, system (2.1) can be written as

$$i\dot{A}_n = f(|A_n|^2)\frac{\partial H}{\partial \overline{A}_n}.$$

System (2.1) has also the constant of motion

$$P = \sum_{n\in\mathbb{Z}} g(|A_n|^2), \tag{2.2}$$

known as the power (or the number, or norm). The Poisson bracket is given as

$$\{\Phi, \Psi\} = -i\sum_{n\in\mathbb{Z}}\left(\frac{\partial\Phi}{\partial A_n}\frac{\partial\Psi}{\partial\overline{A}_n} - \frac{\partial\Phi}{\partial\overline{A}_n}\frac{\partial\Psi}{\partial A_n}\right)f(|A_n|^2),$$

where Φ and Ψ are arbitrary functionals of the variable A_n. As a particular case, we have that

$$\{A_n, \overline{A}_n\} = -if(|A_n|^2),$$

and

$$\{A_n, A_m\} = \{\overline{A}_n, \overline{A}_m\} = 0.$$

With respect to the Poisson bracket, system (2.1) is written in the following form:

$$\dot{A}_n = \{H, A_n\}.$$

Now, let us return to the particular cases of the DNLS systems studied herein.

- *The AL equation* (1.1): It corresponds to the case of system (2.1) for $f(\rho) = 1 + \mu\rho$ and $F(\rho) = -2$. We remark that the integrable AL conserves the momentum

$$M = 2\mathrm{Im}\sum \psi_n \overline{\psi}_{n+1}. \tag{2.3}$$

- *The generalization AL equation* (1.6): It is the case of $f(\rho) = 1 + \mu\rho^\sigma$ and $F(\rho) = -2$.
- *The cubic DNLS equation* (1.5): $f(\rho) = 1$ and $F(\rho) = -2 + \gamma\rho$.
- *The DNLS equation with general power nonlinearity* (1.7): $f(\rho) = 1$ and $F(\rho) = -2 + \gamma\rho^\sigma$.
- *The DNLS equation with saturable nonlinearity* (1.8): $f(\rho) = 1$ and $F(\rho) = -2 + \frac{\gamma}{1+\rho^2}$.

Another important case that we will not study in the present paper is the Salerno model (SM).[25,26] It corresponds to the case of $f(\rho) = 1 + \mu\rho$ and $F(\rho) = -2 + \gamma\rho$, that is, a combination of the AL and DNLS systems. The study of the Salerno model provides information about the intrinsic collapse of localized states in the presence of integrability-breaking terms, in particular, how the reflection symmetry and translational symmetry of the integrable AL are broken by the on-site nonlinearity of the DNLS. The review article[24] highlights the relation between the AL and SM systems and establishes a link between the classical systems considered in the present paper, and their quantum counterparts in the form of Bose–Hubbard models. For the global in time existence of solutions of the SM, we refer to Ref. 10.

For the proof of the main results, which are given in Sec. III, we will explicitly refer to the power (2.2) associated with the generalized G-AL system (1.6). It has a non-trivial functional form provided and studied in Ref. 11 and is a key ingredient for the implementation of the closeness arguments.

III. PROOF OF CLOSENESS OF THE AL AND G-AL SOLUTIONS

The analytical proof of closeness we shall demonstrate concerns the infinite lattice with vanishing boundary conditions. However, we remark that the argument can be easily modified to cover other cases of boundary conditions, such as periodic ones. Consider, then, the initial conditions for the integrable AL (1.1) and the non-integrable G-AL,

$$\psi_n(0) = \psi_{n,0}, \quad n \in \mathbb{Z}, \tag{3.1}$$

and

$$U_n(0) = U_{n,0}, \quad n \in \mathbb{Z}, \tag{3.2}$$

respectively. We start with the statement of the following theorem.

Theorem III.1

a. *We assume that for every* $0 < \varepsilon < 1$, *the initial conditions (3.1) of the AL (1.1) and the initial conditions (3.2) of the G-AL (1.6) satisfy the following:*

$$\|\psi(0) - U(0)\|_{l^2} \le C_0\,\varepsilon^3, \tag{3.3}$$
$$\|U(0)\|_{l^2} \le C_{\delta,0}\,\varepsilon, \tag{3.4}$$
$$P_\mu(0) = \sum_n \ln\left(1 + \mu|\psi_n(0)|^2\right) \le \ln\left(1 + (C_{\mu,0}\,\varepsilon)^2\right), \tag{3.5}$$

for some constants $C_0, C_{\delta,0}, C_{\mu,0} > 0$. *Then, for arbitrary* $T_f > 0$, *there exists a constant* $C = C(\delta, \mu, C_{\mu,0}, C_{\delta,0}, T_f, \sigma)$ *such that the corresponding solutions for every* $t \in [0, T_f]$, *satisfy the estimate*

$$\|y(t)\|_{l^2} = \|\psi(t) - U(t)\|_{l^2} \le C\varepsilon^3. \tag{3.6}$$

b. *Under assumptions* (3.4) and (3.5), *for every* $0 < \varepsilon < 1$ *and* $t \in [0, T_f]$, *the maximal distance* $\|y(t)\|_{l^\infty} = \sup_{n\in\mathbb{Z}} |y_n(t)| = \sup_{n\in\mathbb{Z}} |\psi_n(t) - U_n(t)|$ *between individual units of the systems satisfies the estimate*

$$\|y(t)\|_{l^\infty} \le C\varepsilon^3. \tag{3.7}$$

Proof. For simplicity, we set $\kappa = \nu = 1$. The corresponding evolution equation for the local distance $y_n = \psi_n - U_n$ reads

$$i\dot{y}_n = \Delta_d y_n + \left[\mu|\psi_n|^2(\psi_{n+1} + \psi_{n-1}) - \delta\,|U_n|^{2\sigma}(U_{n+1} + U_{n-1})\right], \tag{3.8}$$

where $\Delta_d y_n = y_{n+1} - 2y_n + y_{n-1}$ is the 1D discrete Laplacian. Let us recall that when $u_n \in \mathbb{C}$, the space $l^2(\mathbb{Z};\mathbb{C})$ becomes a real Hilbert space, $l^2(\mathbb{Z};\mathbb{C}) \equiv l^2(\mathbb{Z};\mathbb{R}) \times l^2(\mathbb{Z}^N;\mathbb{R})$, if endowed with the real inner product

$$(u, v)_{l^2} = \mathrm{Re}\sum_{n\in\mathbb{Z}^N} u_n\bar{v}_n.$$

In this setting, the operator $\Delta_d : l^2 \to l^2$ is bounded and self-adjoint,

$$(\Delta_d u, v)_{l^2} = (u, \Delta_d v)_{l^2}, \quad u,\ v \in l^2,$$
$$\|\Delta_d u\|_{l^2}^2 \le 4\|u\|_{l^2}^2.$$

Moreover, it satisfies

$$(\Delta_d u, u)_{l^2} = -\sum_{n\in\mathbb{Z}}|u_{n+1} - u_n|^2 \le 0 \text{ for all } u \in l^2. \tag{3.9}$$

When multiplying Eq. (3.8) by $\bar{y}_n$, summing over $\mathbb{Z}$, and keeping the imaginary parts, we may use (3.10) and get that

$$\frac{1}{2}\frac{d}{dt}\|y(t)\|_{l^2}^2 = \mu\mathrm{Im}\sum_{n\in\mathbb{Z}}\left[|\psi_n|^2(\psi_{n+1} + \psi_{n-1})\right]\bar{y}_n - \delta\mathrm{Im}\sum_{n\in\mathbb{Z}}\left[|U_n|^{2\sigma}(U_{n+1} + U_{n-1})\right]\bar{y}_n. \tag{3.10}$$

To estimate the terms on the right-hand side of (3.10), we use the Cauchy–Schwarz inequality and the continuous embeddings

$$l^r \subset l^s, \quad \|\phi\|_{l^s} \le \|\phi\|_{l^r}, \quad 1 \le r \le s \le \infty. \tag{3.11}$$

For the first term on the right-hand side of (3.10), we get

$$\begin{aligned}\left|\mathrm{Im}\sum_{n\in\mathbb{Z}}\left[|\psi_n|^2(\psi_{n+1} + \psi_{n-1})\right]\bar{y}_n\right| &\le 2\sup_{n\in\mathbb{Z}}|\psi_n|\sum_{n\in\mathbb{Z}^N}|\psi_n|^2\,|\bar{y}_n| \\ &\le 2\left(\sup_{n\in\mathbb{Z}}|\psi_n|\right)^2\sum_{n\in\mathbb{Z}^N}|\psi_n|\,|\bar{y}_n| \le 2\left(\sup_{n\in\mathbb{Z}^N}|\psi_n|\right)^2\|\phi\|_{l^2}\|y\|_{l^2} \\ &\le 2\|\psi\|_{l^2}^3\|y\|_{l^2}.\end{aligned} \tag{3.12}$$

For the second term on the right-hand side of (3.10), we obtain

$$\begin{aligned}\left|\mathrm{Im}\sum_{n\in\mathbb{Z}}\left[|U_n|^{2\sigma}(U_{n+1} + U_{n-1})\right]\bar{y}_n\right| &\le 2\sup_{n\in\mathbb{Z}}|U_n|\sum_{n\in\mathbb{Z}^N}|U_n|^{2\sigma}\,|\bar{y}_n| \\ &\le 2\left(\sup_{n\in\mathbb{Z}}|U_n|\right)^{2\sigma}\sum_{n\in\mathbb{Z}^N}|U_n|\,|\bar{y}_n| \le 2\left(\sup_{n\in\mathbb{Z}^N}|U_n|\right)^{2\sigma}\|U\|_{l^2}\|y\|_{l^2} \\ &\le 2\|U\|_{l^2}^{2\sigma+1}\|y\|_{l^2}.\end{aligned} \tag{3.13}$$

Then, from (3.10)–(3.13), we get the inequality

$$\frac{1}{2}\frac{d}{dt}\|y(t)\|_{l^2}^2 \le 2\left(\mu\|\psi\|_{l^2}^3 + \delta\|U\|_{l^2}^{2\sigma+1}\right)\|y(t)\|_{l^2}. \tag{3.14}$$

Inequality (3.14), when combined with $\frac{d}{dt}\|y(t)\|_{l^2}^2 = 2\|y(t)\|_{l^2}\frac{d}{dt}\|y(t)\|_{l^2}$, implies that

$$\frac{d}{dt}\|y(t)\|_{l^2} \le 2\left(\gamma\|\psi\|_{l^2}^3 + \delta\|U\|_{l^2}^{2\sigma+1}\right). \tag{3.15}$$

For the solutions of the AL, the *deformed* norm

$$P_\mu(t) = \sum_n \ln(1+\mu|\psi_n|^2)$$

is conserved, that is,

$$P_\mu(t) = P_\mu(0). \tag{3.16}$$

This conservation implies the following bound (see Ref. 10, Lemma II.1 and Ref. 15):

$$\|\psi(t)\|_{l^2}^2 \le \exp(P_\mu(0)) - 1 \le C_{0,\mu}^2\varepsilon^2, \qquad \forall t \ge 0. \tag{3.17}$$

On the other hand, the G-AL has a nontrivial conservation law,[11]

$$P_\delta(t) = \sum_{n\in\mathbb{Z}}|U_n|^2\,{}_2F_1\left(1, \frac{1}{\sigma}, 1+\frac{1}{\sigma}; -|U_n|^{2\sigma}\right), \tag{3.18}$$

where ${}_2F_1(a,b,c;\,z)$ is the Gauss hypergeometric function for $a,b,c,z \in \mathbb{C}$. We recall that

$${}_2F_1(a,b,c;z) = 1 + \frac{ab}{c}z + \frac{a(a+1)b(b+1)}{c(c+1)2!}z^2 + \cdots \tag{3.19}$$

on the disk $|z| < 1$ and by analytic continuation outside this disk.

By using the expansion (3.19) for the term ${}_2F_1\left(1, \frac{1}{\sigma}, 1+\frac{1}{\sigma}; -|U_n|^{2\sigma}\right)$ of the quantity (3.18) and its conservation, as well as the embedding relation (3.11) for $r = 2$ and $s = 2\sigma$, we may derive the following inequality for small values of $\|U\|_{l^2} = \left(\sum_{n\in\mathbb{Z}}|U|^2\right)^{\frac{1}{2}}$:

$$\begin{aligned}\sum_{n\in\mathbb{Z}}|U_n(t)|^2 + \mathcal{O}\left(\sum_{n\in\mathbb{Z}}|U_n(t)|^{2\sigma}\right) &= \sum_{n\in\mathbb{Z}}|U_n(0)|^2 + \mathcal{O}\left(\sum_{n\in\mathbb{Z}}|U_n(0)|^{2\sigma}\right)\\ &\le \sum_{n\in\mathbb{Z}}|U_n(0)|^2 + \mathcal{O}\left(\left(\sum_{n\in\mathbb{Z}}|U_n(0)|^2\right)^{\sigma}\right)\\ &\le C_{\delta,0}^2\varepsilon^2 + \mathcal{O}(\varepsilon^{2\sigma}),\end{aligned} \tag{3.20}$$

for which we have also used the smallness assumption (3.4) on the initial data. Hence, under these assumptions, we deduce the estimate

$$\|U(t)\|_{l^2}^2 \le \hat{C}_{0,\sigma,\delta}^2\varepsilon^2 + \mathcal{O}(\varepsilon^{2\sigma}), \tag{3.21}$$

where $\hat{C}_{0,\sigma,\delta}$ will stand for a general constant depending on σ and $C_{\delta,0}$. Then, using (3.17) and (3.21) in the differential inequality (3.15), we get that

$$\frac{d}{dt}\|y(t)\|_{l^2} \le 2\left(\mu C_{0,\mu}^3 + \delta\hat{C}_{0,\delta,\sigma}^{2\sigma+1}\right)\varepsilon^3. \tag{3.22}$$

Integrating the inequality (3.22) in the arbitrary interval $[0, T_f]$ and using the assumption (3.3) on the distance $\|y(0)\|_{l^2} = \|\psi(0) - U(0)\|_{l^2}$ of the initial data, we obtain that

$$\|y(t)\|_{l^2} \leq 2\left(\mu C_{0,\mu}^3 + \delta \hat{C}_{0,\sigma,\delta}^{2\sigma+1}\right) T_f \varepsilon^3 + \|y(0)\|_{l^2}$$
$$\leq 2\left(\mu C_{0,\mu}^3 + \delta \hat{C}_{0,\sigma,\delta}^{2\sigma+1}\right) T_f \varepsilon^3 + C_0 \varepsilon^3.$$

Hence, for the constant

$$C = 2\left(\mu C_{0,\mu}^3 + \delta \hat{C}_{0,\sigma,\delta}^{2\sigma+1}\right)\Big) T_f + C_0, \tag{3.23}$$

we conclude with the claimed estimate (3.6).

b. The result is an immediate consequence of embedding (3.11) and estimate (3.6) since $\|y(t)\|_{l^\infty} \leq \|y(t)\|_{l^2}$. □

Remark III.1 As in Ref. 10, we should also remark herein, that the Proof of Theorem III.1 establishes that the growth rate of the distance $\|y(t)\|_{l^2}$ is uniformly bounded for any $0 < \epsilon < 1$ and $t \in (0, \infty)$, that is,

$$\frac{d}{dt}\|y(t)\|_{l^2} \leq K \varepsilon^3, \tag{3.24}$$

where the constant K depends only on the parameters and the initial conditions, but not on t. Therefore, the distance of solutions grows at most linearly for any $t \in (0, \infty)$ according to the estimate

$$\|y(t)\|_{l^2} \leq M t \varepsilon^3, \tag{3.25}$$

and similarly for the case of the l^∞-distance,

$$\|y(t)\|_{l^\infty} \leq K_1 t \varepsilon^3, \quad \forall \quad t \in (0, \infty), \tag{3.26}$$

with the constant K_1 bearing a similar dependence as M. Such linear growth rates as (3.24) and (3.26) have been proved particularly relevant in the context of nonlinear PDEs. We refer to the time-growth estimates for the relevant distant function between the solutions, when the NLS is consdidered as the inviscid limit of the Ginzburg–Landau PDE.[21] In such limits, the distance functions may grow even exponentially with respect to time.[22]

As the momentum M (2.3) is conserved only by the integrable AL system (1.1), having the closeness result of Theorem III.1 in hand, we may estimate the difference of momenta between the solutions of the integrable AL (1.1) and its non-integrable generalization (1.6).

Corollary III.1. Assume that the conditions of Theorem III.1 *are satisfied. Then, for arbitrary $T_f > 0$, the difference of momenta ΔM between the solutions of the integrable AL (1.1) and (1.6) satisfies for every $T \in [0, T_f]$, the estimate*

$$\Delta M(t) \leq C\varepsilon^4 \tag{3.27}$$

for some constant $C > 0$ depending on the same parameters and T_f as the constant C given in Theorem III.1.

Proof. We denote by

$$M_{AL}(t) = 2\mathrm{Im}\sum_{n\in\mathbb{Z}} \psi_n(t)\overline{\psi}_{n+1}(t)$$

the momentum associated with the solutions of the AL lattice (1.1) and by

$$M_{GAL}(t) = 2\mathrm{Im}\sum_{n\in\mathbb{Z}} U_n(t)\overline{U}_{n+1}(t)$$

the momentum associated with the G-AL lattice (1.6). Then, the difference $\Delta M = M_{AL} - M_{GAL}$ can be written as

$$\Delta M = 2\mathrm{Im}\sum_{n\in\mathbb{Z}} \psi_n\left(\overline{\psi}_{n+1} - \overline{U}_{n+1}\right) + 2\mathrm{Im}\sum_{n\in\mathbb{Z}} \overline{U}_{n+1}(\psi_n - U_n).$$

Then, by using the Cauchy–Schwarz inequality and the estimates (3.17) for ψ and (3.21) for U and (3.6) for $y = \psi - U$, we get that

$$\begin{aligned} |\Delta M| &\le 2\|\psi\|_{l^2}\|\psi - U\|_{l^2} + 2\|U\|_{l^2}\|\psi - U\|_{l^2} \\ &\le 2C\, C_{0,\mu}\varepsilon^4 + 2C\,\hat{C}_{0,\sigma,\delta}\varepsilon^4 \\ &\le C\varepsilon^4, \end{aligned}$$

and the proof is completed. □

IV. NUMERICAL RESULTS

A. Persistence of the AL-soliton in the G-AL lattice

In this section, we present a study of the generalized G-AL lattice (1.6) in the cubic case $\sigma = 2$ similar to the one presented in Ref. 10 for the dynamics of the AL-soliton. As the initial condition, we use the one-soliton solution of the AL equation (1.3),

$$\begin{aligned} U_n(0) &= \psi_n^s(0) \\ &= \frac{\sinh\beta}{\sqrt{\mu}}\operatorname{sech}(\beta n)\exp(i\alpha n), \quad n \in \mathbb{Z}, \end{aligned} \tag{4.1}$$

$$\|\psi^s(0)\|_{l^2} = \|U(0)\|_{l^2} = \varepsilon, \tag{4.2}$$

where $\alpha \in [-\pi, \pi]$ and $\beta \in [0, \infty)$. In order to comply with the smallness condition (4.2), we choose the parameter values accordingly so that persistence of the corresponding AL-soliton in the DNLS can be expected.

Figure 1 depicts the spatiotemporal evolution of the density $|U_n(t)|^2$ of the soliton initial condition when $\mu = 1$, $\alpha = \pi/10$, and $\beta = \operatorname{arcsinh}(0.02)$ for the G-AL equation (1.6) with $\delta = 1$. The evolution is shown for the time span $t \in [0, 2500]$ ($T_f = 2500$) and for a chain of $K = 2400$ units with periodic boundary conditions. The evolution of the soliton in the G-AL depicted in the top-left panel of Fig. 1 confirms the persistence of the AL-soliton with amplitude of order $\mathcal{O}(\varepsilon)$. Notably, persistence lasts for a significant large time interval, particularly when one has in mind that our analysis is a "continuous dependence on the initial data result" *where, generally, the time interval of such a dependence on the initial data for a given equation might be short*. Note that for this example of initial condition, the value of its l^2-norm (4.2) is $\varepsilon = 0.2$.

Our numerical results confirm convincingly the analytical predictions presented by Theorem III.1, concerning the distance

$$y(t) = U(t) - \psi(t),$$

between the solutions of the AL and the G-AL. The top-right panel of Fig. 1 depicts the time evolution of $\|y(t)\|_{l^2}$, and the bottom-left panel depicts the evolution of $\|y(t)\|_{l^\infty}$, corresponding to the dynamics of the quintic G-AL shown in the top-left panel of Fig. 1. The time evolution of the norm of the distance function is plotted with a green solid curve. Both panels illustrate the qualitative and quantitative relevance of the growth estimates (3.24)–(3.26). Note that since $U(0) = \psi(0)$, the constant C on the estimates (3.6) and (3.7) reads as

$$C = 2\left(\mu C_{0,\mu}^3 + \hat{C}_{0,\sigma,\delta}\right)T_f.$$

Since the considered example of the initial condition $\epsilon \sim \mathcal{O}(10^{-1})$ and the time of integration is of order $T_f \sim \mathcal{O}(10^3)$, the constant C should be of the order $C \sim \mathcal{O}(1)$. Then, according to the analytical estimates, one has for this large T_f

$$\|y(t)\|_{l^\infty} \le \|y(t)\|_{l^2} \le C\varepsilon^3 \sim \mathcal{O}(1), \quad t \in [0, T_f].$$

The corresponding panels of Fig. 1 reveal that the numerical order is significantly lower: $\|y(t)\|_{l^2} \sim O(10^{-1})$, for $t \in [0, T_f]$. The variation of $\|y(t)\|_{l^\infty}$ is even of smaller order as shown in the bottom panel, showing that $\|y(t)\|_{l^\infty} \sim \mathcal{O}(10^{-2})$.

For the numerical time-growth rate of $\|y(t)\|_{l^2}$, it holds that

$$\frac{d}{dt}\|y(t)\|_{l^2} \sim \mathcal{O}(10^{-4}), \quad t \in [0, T_f],$$

which is yet of lower order than the corresponding analytical prediction $\mathcal{O}(10^{-3})$.

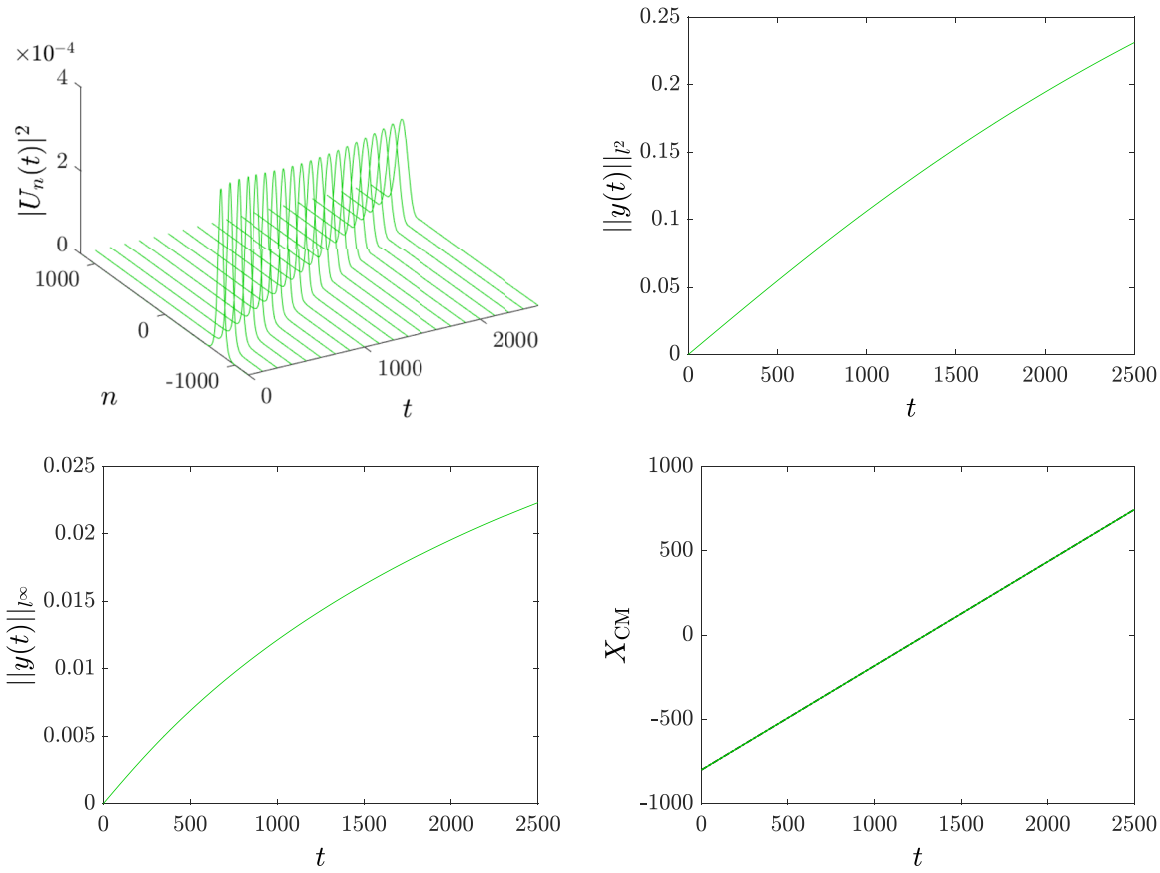

FIG. 1. Top-left panel: spatiotemporal evolution of the initial condition (4.1) in the G-AL lattice with $\delta = 1$ for the quintic non-linearity $\sigma = 2$. Parameters of the initial condition $\alpha = \pi/10$ and $\beta = \operatorname{arcsinh}(0.02)$, $\mu = 1$. Top-right panel and bottom-left panel: time evolution of $\|y(t)\|_{l^2}$ and $\|y(t)\|_{l^\infty}$, respectively, corresponding to the soliton dynamics shown in the top-left panel (details in the text of Sec. IV). Bottom-right panel: space time evolution of the soliton center $X_{\mathrm{CM}} = (\sum_n n|\phi_n|^2)/(\sum_n|\phi_n|^2)$ for the AL (1.1) (black dashed-dotted line) and G-AL (1.6) (green continuous line).

The bottom-right panel of Fig. 1 depicts the preservation of the soliton's velocity in the G-AL lattice as the corresponding curves for the G-AL evolution (green curve) and the analytical soliton (black curve) are indistinguishable. For the considered value of β, we have $\sinh(\beta) \approx \beta$ so that the soliton's speed is $c = 2\sin(\alpha) = 0.6181$.

B. The study of the evolution of the AL-soliton in the DNLS

1. The quintic DNLS

The same excellent agreement with the analytical predictions for the persistence of the AL-soliton is observed in the case of the generalized DNLS with the power nonlinearity (1.7),

$$i\dot{\phi}_n + \kappa\nu(\phi_{n+1} - 2\phi_n + \phi_{n-1}) + \gamma|\phi_n|^{2\sigma}\phi_n = 0, \quad n \in \mathbb{Z}, \quad \gamma \in \mathbb{R}, \quad \sigma > 0. \tag{4.3}$$

The analogous result to Theorem III.1 was proved in Ref. 10 even for higher-dimensional DNLS lattices, which is recalled herein for the sake of completeness.

Theorem IV.1

A. *Assume that $\sigma > 0$ and that for every $\varepsilon > 0$, the initial conditions of the AL lattice (1.1) and DNLS equation (4.3) satisfy*

$$\|\phi(0) - \psi(0)\|_{l^2} \le C_0\, \varepsilon^3, \tag{4.4}$$

$$\|\phi(0)\|_{l^2} \le C_{\gamma,0}\, \varepsilon, \tag{4.5}$$

$$P_\mu(0) = \sum_{n\in\mathbb{Z}^N} \ln(1 + \mu|\psi_n(0)|^2) \le \ln(1 + (C_{\mu,0}\, \varepsilon)^2), \tag{4.6}$$

for some constants $C_0, C_{\gamma,0}, C_{\mu,0} > 0$. *Then, for arbitrary* $T_f > 0$, *there exists a constant* $C = C(\gamma,\ \mu, C_{\mu,0}, C_{\gamma,0}, T_f)$ *such that the corresponding solutions for every* $t \in [0, T_f]$ *satisfy the estimate*

$$\|y(t)\|_{l^2} = \|\phi(t) - \psi(t)\|_{l^2} \le C\, \varepsilon^3. \tag{4.7}$$

B. Under assumptions (4.4)–(4.6), for every $\varepsilon > 0$ and $t \in [0, T_f]$, the maximal distance $\|y(t)\|_{l^\infty} = \sup_{n\in\mathbb{Z}^N} |y_n(t)| = \sup_{n\in\mathbb{Z}^N} |\psi_n(t) - \phi_n(t)|$ satisfies the estimate

$$\|y(t)\|_{l^\infty} \le C\varepsilon^3. \tag{4.8}$$

In Fig. 2, we present the numerical results for the evolution of the AL-soliton initial condition (4.1) and (4.2) in the quintic DNLS (4.3) with $\sigma = 2$ and $\gamma = 1$. We observe that the dynamics are almost identical to the evolution of the generalized G-AL lattice. Still,

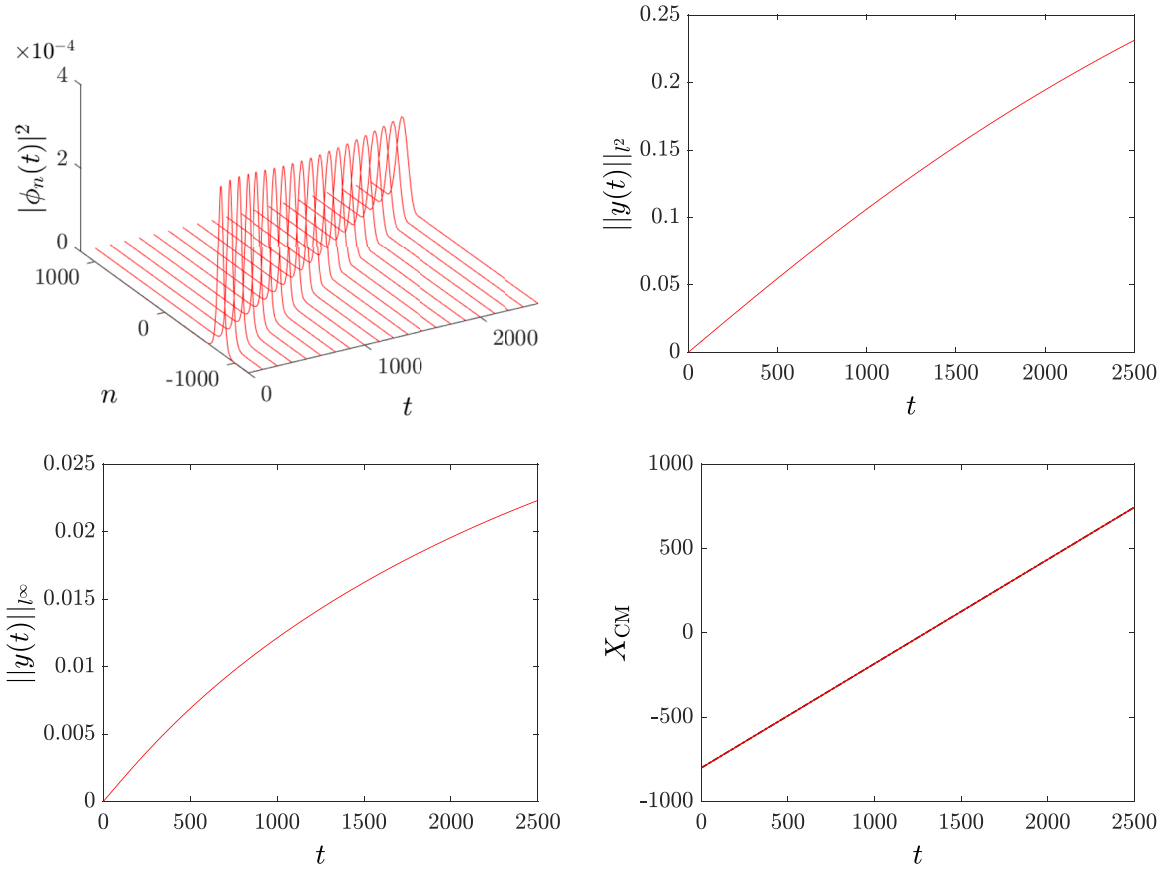

FIG. 2. Top-left panel: spatiotemporal evolution of the initial condition (4.1) in the quintic DNLS lattice (4.3) with $\sigma = 2$ and $\gamma = 1$. Parameters of the initial condition $\alpha = \pi/10$ and $\beta = \text{arcsinh}(0.02)$, $\mu = 1$. Top-right panel and bottom-left panel: time evolution of $\|y(t)\|_{l^2}$ and $\|y(t)\|_{l^\infty}$, respectively, corresponding to the soliton dynamics shown in the top-left panel (details in the text of Sec. IV). Bottom-right panel: space time evolution of the soliton center $X_{\text{CM}} = (\sum_n n|\phi_n|^2)/(\sum_n |\phi_n|^2)$ for the AL (1.1) (black dashed-dotted line) and the quintic DNLS (4.3) (red continuous line).

this excellent agreement with the analytical predictions of the associated Theorem IV.1 is explained by the very similar functional expression for the the constant C in the estimates (4.7) and (4.8) as in Theorem III.1 for the G-AL lattice. This coincidence of the constants explains the same rates of growth in the evolution of the norms of the distance function $y(t)$.

2. The cubic DNLS: Evolution of higher amplitude AL-soliton

To test the limits of our analytical predictions on the persistence of small amplitude AL-solitons, we present in this paragraph, the results of a numerical study concerning the evolution of the AL-initial condition for a higher initial amplitude, corresponding to the case $\beta = \text{arcsinh}(0.1)$. For this choice of the initial condition, the value of the l^2-norm (4.2) of the initial condition is $\varepsilon = 0.4$.

The top panels of Fig. 3 show the spatiotemporal evolution of the AL-soliton initial condition described above in the cubic DNLS lattice (4.3) $\sigma = 1$ with $\gamma = 1$. In the top-left panel, the evolution is shown for $t \in [0, 2500]$, i.e., $T_f = 2500$ and for a lattice of $K = 2400$ units. The top-right panel shows the evolution for $t \in [0, 1000]$, i.e., $T_f = 10\,000$, for a lattice of $K = 7200$ units. We still observe the evolution of a solitonic structure, which, however, exhibits different dynamical features as the results of the top-right panel reveal: the AL-initial condition evolves as a large period-spatially localized breather.

The bottom panels of Fig. 3 show the evolution of the same AL-soliton initial condition for the quintic DNLS (4.3) $\sigma = 2$ and the remaining parameters are fixed as in the top panels. In this case, the evolution of the AL-initial condition exhibits a self-similar decay of its initial amplitude, accompanied by an increase of its localization width. The dynamics tend to achieve a small amplitude solitonic asymptotic state of large width; the norm of the solution cannot converge to zero as the system is conservative preserving the initial norm $\|\phi(0)\|_{l^2}$.

We remark that the observation of the above dynamical features is in agreement with the character of the analytical results based on the continuous dependence of solutions on the initial data: the observed features in Fig. 3 occur after the finite time interval where the corresponding solutions remain close in profile and amplitude. As displayed in Fig. 4, for $t \in [0, 50]$ in the cubic case and for $t \in [0, 20]$ in the quintic case, the deformations emerging from the initial AL-one soliton in amplitude and profiles are incremental.

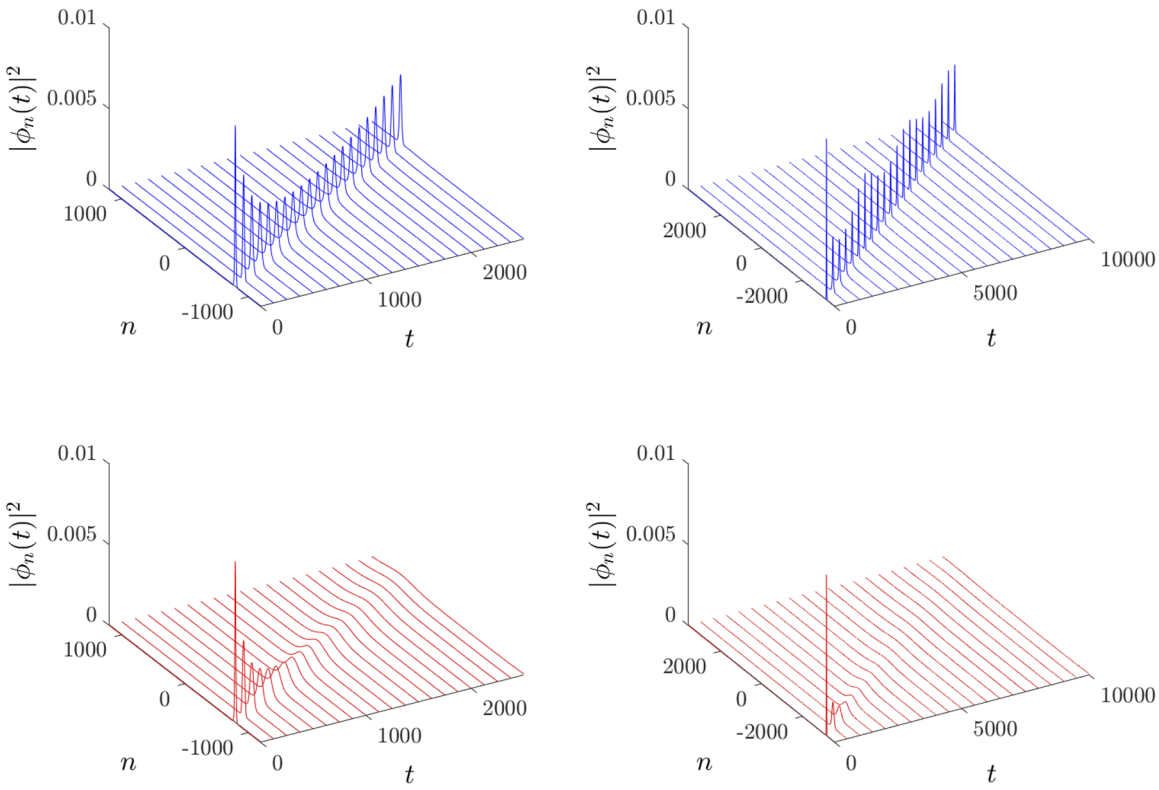

FIG. 3. Top-left panel: spatiotemporal evolution of the initial condition (4.1) in the cubic DNLS lattice (4.3) with $\sigma = 1$ and $\gamma = 1$, for $t \in [0, T_f] = [0, 2500]$, in a lattice of $K = 2400$ units. Parameters of the initial condition $\alpha = \pi/10$ and $\beta = \text{arcsinh}(1)$, $\mu = 1$. Top-right panel: the same evolution for $t \in [0, T_f] = [0, 10\,000]$ and for a chain of $K = 7200$ units. Bottom panels: the spatiotemporal evolution of the of the initial condition (4.1) with $\alpha = \pi/10$ and $\beta = \text{arcsinh}(1)$, $\mu = 1$ in the case of the quintic DNLS lattice (4.3), and $\sigma = 2$. Rest of the parameters are as in the bottom panels.

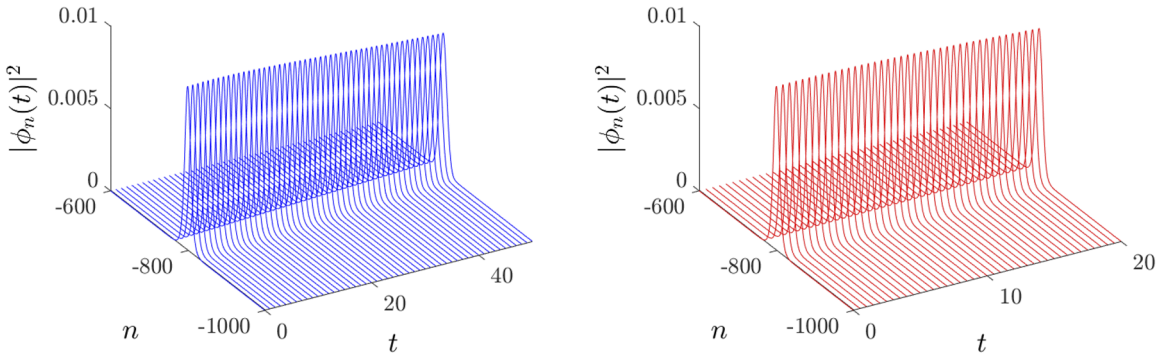

FIG. 4. Same as Fig. 3 but focusing on the time-interval $t \in [0, T_f] = [0, 50]$ for $K = 2400$ units.

The above effects can also be found in the time evolution of the norms of the corresponding distance functions $y(t)$ shown in Fig. 5. Note the time oscillations of the relevant metrics in the case of the cubic DNLS $\sigma = 1$ (blue solid line curves) and a decaying oscillatory behavior in the case of the quintic DNLS $\sigma = 2$ (red dashed curves). Remarkably, the analytical estimates are still fulfilled and the illustrated evolution does not contradict the analytical predictions even for large time intervals. Studying the case $T_f = 10\,000$, which is of order $\mathcal{O}(10^4)$ and for the

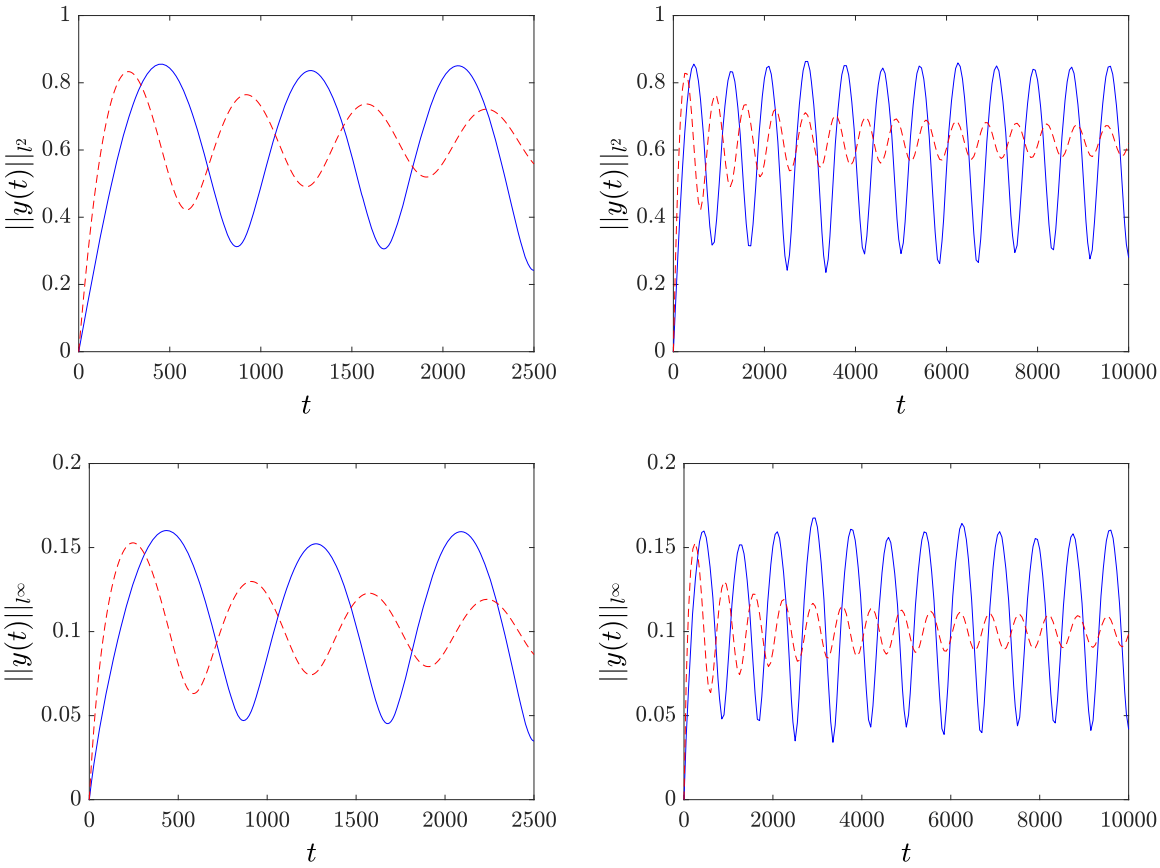

FIG. 5. Top-left panel: evolution of $\|y(t)\|_{l^2}$ associated with the spatiotemporal evolution in the cubic DNLS (4.3) $\sigma = 1$—blue continuous curve—and the quintic DNLS (4.3) $\sigma = 2$—red dashed curve—when $t \in [0, 2500]$ and $K = 2400$ lattice units. Top-right panel: evolution of $\|y(t)\|_{l^2}$ associated with the spatiotemporal evolution in the cubic DNLS (4.3) $\sigma = 1$—blue continuous curve—and the quintic DNLS (4.3) $\sigma = 2$—red dashed curve—when $t \in [0, 10\,000]$ and $K = 7200$ lattice units. Bottom panels: the same as above but for $\|y(t)\|_{l^\infty}$.

initial norm $\|\phi(0)\|_{l^2} = \epsilon \sim \mathcal{O}(10^{-1})$, the analytical prediction for the upper-bound of the metrics is again satisfied: In particular, the results depicted in Fig. 5 support the fact that the metric $\|y(t)\|_{l^2}$ gets altered from order $\mathcal{O}(10^{-1})$ to $\mathcal{O}(1)$ and is of order $\mathcal{O}(10^{-1})$ in the case of $\|y(t)\|_{l^\infty}$.

As shown in Fig. 6 depicting the evolution of the center of the solitons, the velocity of the AL-soliton is again preserved in large time intervals for the case of $\beta = \text{arcsinh}(0.1)$. For example, in the quintic DNLS of $K = 7200$ units, the divergence starts at $t \sim 8000$; the persistence of the trace justifies that in the case of the quintic DNLS, the asymptotic state resulting from the initial condition should be a small amplitude, self-similarly deformed soliton, as explained above.

Concerning the evolution of momenta, we remark that Corollary III.1 remains valid for the DNLS models.

C. Closeness of the momentum

Figure 7 represents the numerical results of a numerical study on the time evolution of the error of the momenta

$$|\Delta M(t)| = |M_{AL}(t) - M_{NI}(t)|,$$

discussed in Corollary III.1; M_{IN} stands for the momentum of the solutions of the non-integrable lattices. The top-left panel of Fig. 7 plots $|\Delta M(t)|$ for the dynamics of the 1-soliton initial condition (4.1) displayed in Fig. 1 for the G-AL lattice (1.6). The top-right panel of Fig. 7 plots $|\Delta M(t)|$ for the dynamics of the 1-soliton initial condition discussed in Fig. 2 for the quintic DNLS (4.3) with $\sigma = 2$. The bottom panels of Fig. 7 plot $|\Delta M(t)|$ for the 1-soliton dynamics discussed in Fig. 3 for the initial condition of larger amplitude. Again, we observe excellent agreement of the numerical results with the analytical predictions for the closeness of the momenta predicted by Corollary III.1, since $|\Delta M(t)| \sim \mathcal{O}(10^{-4})$ or of order $\mathcal{O}(10^{-3})$.

D. AL-peregrine soliton in DNLS and generalized AL-systems

We conclude the presentation of the numerical results with what we think is one of the most striking applications of our approach: the persistence of small amplitude rational solutions possessing the functional form of the discrete Peregrine soliton (1.4) of the integrable AL lattice, in the non-integrable G-AL and DNLS systems. We present the results for the quintic G-AL (1.6) with $\sigma = 2$, the cubic DNLS (4.3) with $\sigma = 1$, and the saturable DNLS with the nonlinearity (1.8); for the saturable DNLS, the proof of the variant of Theorem IV.1 is also given in Ref. 10, Sec. V, pg. 357. We remark that the analytical results on the closeness of solutions can be straightforwardly adapted to cover the case of the periodic boundary conditions. The latter are suitable to simulate the behavior of solutions on top of a finite background such as in the case the AL-PS (1.4).

For the numerical simulations, since the systems are autonomous and are invariant under the transformation $t \to -t$, we use as the initial condition the AL-analytical Peregrine soliton (1.4) at some $t = t_0 < 0$,

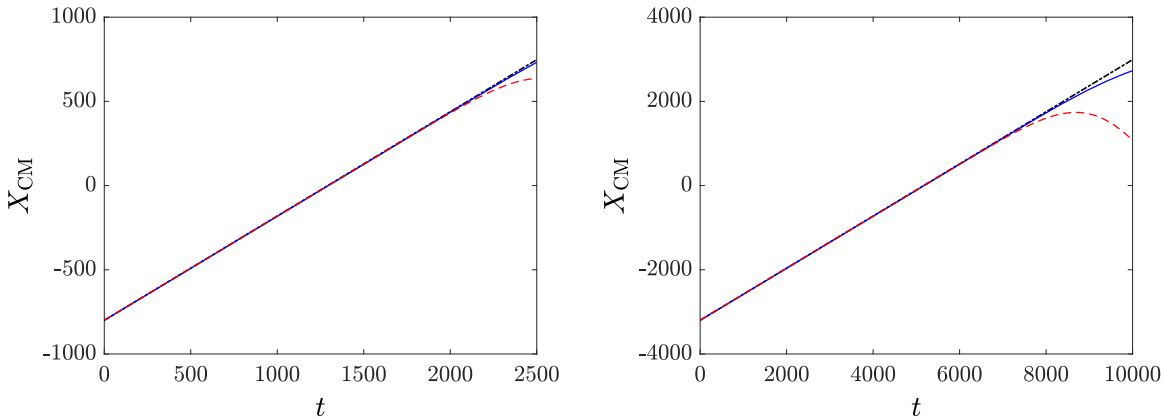

FIG. 6. Space time evolution of the soliton center $X_{CM} = (\sum_n n|\phi_n|^2)/(\sum_n |\phi_n|^2)$ for the AL (1.1) (black dashed-dotted curve), the cubic DNLS (4.3) $\sigma = 1$ (blue continuous curve), and the quintic DNLS (4.3) $\sigma = 2$ (red continuous curve), corresponding to the spatiotemporal evolution of the AL-soliton initial condition of Fig. 5 ($\beta = \text{arcsinh}0.1$). Left panel: for the lattices of $K = 2500$ units and $t \in [0, 2500]$. Right panel: for the lattices of $K = 7200$ units and $t \in [0, 10\,000]$.

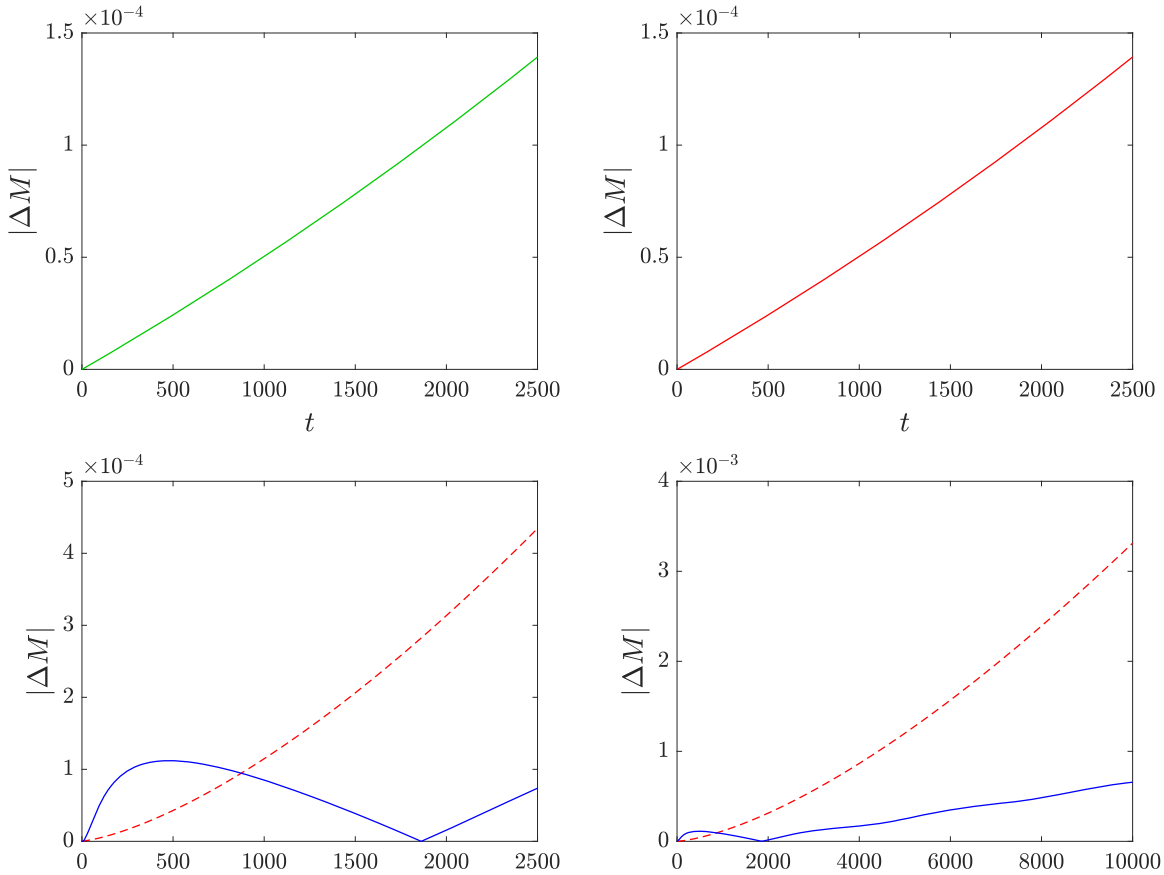

FIG. 7. Top-left panel: the time evolution of the difference $|\Delta M|$ between the momenta of the soliton initial condition (4.1) for the AL system and the G-AL system with the quintic non-linearity $\sigma = 2$ (see Fig. 1). Top-right panel: the same evolution but comparing the AL system against the DNLS lattice with $\sigma = 2$ (see Fig. 2). Bottom-left panel: the same evolution corresponding to the study for the cubic DNLS $\sigma = 1$ [upper (blue) curve] and the quintic DNLS $\sigma = 2$ [lower (red) curve]) of Fig. 3. Bottom-right panel: the same evolution as in the bottom-left panel but for $t \in [0, 1000]$.

$$U_n(t_0) = \phi_n(t_0) = \psi_n^r(t_0)$$
$$= q\left[1 - \frac{4(1+q^2)(1+4iq^2t_0)}{1+4n^2q^2+16q^4t_0^2(1+q^2)}\right]e^{2iq^2t_0}, \quad n \in \mathbb{Z}, \quad t_0 < 0. \tag{4.9}$$

We recall that the analytical Peregrine (1.4) achieves its maximum amplitude at $t = 0$. To be in conformity with a smallness condition for the initial amplitude, we select $q = 0.1$ and set the initial condition at $t_0 = -50$.

Figure 8 shows the spatiotemporal evolution of the density $|U_n(t)|^2$ for the initial condition (4.9) in the quintic G-AL (left panel) and the cubic DNLS (right panel), while the case of the saturable DNLS is depicted in the bottom panel. The results demonstrate the persistence of the Peregrine waveforms of small amplitude in all of the non-integrable lattices. In particular, we note that the evolving waveforms maintain the characteristic spatiotemporal localization of the discrete Peregrine soliton.

Figure 9 portrays the evolution of the norms of the relevant distance functions $y(t)$, confirming once more the closeness analytical results. In the case of the quintic G-AL, the evolution of the norms is plotted with the green dashed-dotted curve, in the case of the cubic DNLS, it is plotted with the blue solid curve, and in the case of the saturable DNLS, it is plotted with the red dashed curve. We observe that in the case of the quintic G-AL, the norms increase incrementally. This should be an effect due to the fact that both systems have a non-local nonlinearity, leading to the fact that the solutions remain closer in comparison with the cases of local nonlinearities. In the case of the cubic DNLS, the maximum for both is of order $\mathcal{O}(10^{-2})$. In the case of the saturable DNLS, the maximum of the l^2-norm is of order $\mathcal{O}(10^{-1})$ and of order $\mathcal{O}(10^{-2})$ for the l^∞-norm, fulfilling in an excellent manner the analytical predictions. The relatively larger magnitude variations of the metrics observed for the saturable DNLS can be explained by the specific functional form of the nonlinearity, which saturates higher amplitudes. Nevertheless, while at first-glance, these features could be considered as counter-intuitive for this type of nonlinearity, the

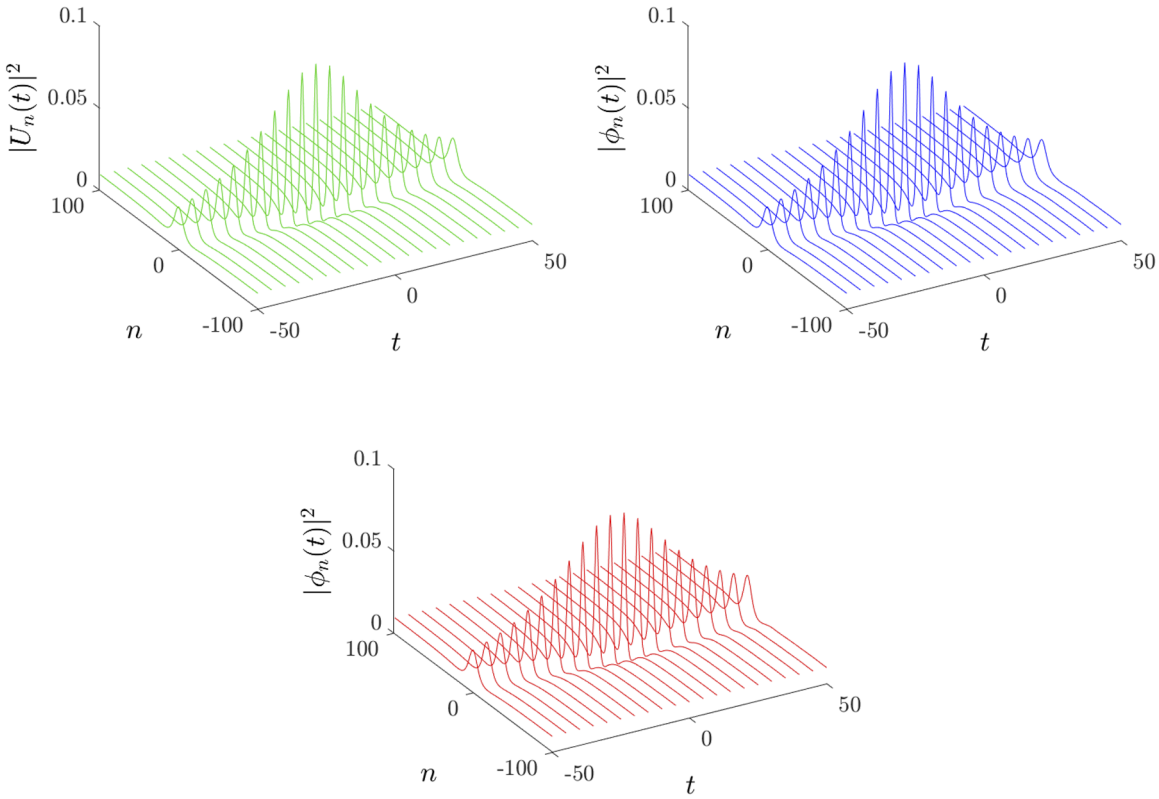

FIG. 8. Left panel: evolution of the rational Peregrine initial condition (4.9) with $q = 0.1$ in the quintic G-AL lattice (1.6) $\sigma = 2$, with $\delta = 1$, for $K = 200$ units and $t \in [-50, 50]$. Right panel: the same evolution in the cubic DNLS (4.3) $\sigma = 1$ when $\gamma = 1$. Rest of the parameters are as in the left panel. Bottom panel: the same evolution in the DNLS with the saturable nonlinearity when $\gamma = 1$. Rest of the parameters are as in the left panel.

analytical results, further corroborated by the numerical studies, confirm that Peregrine-type waveforms close to the analytical ones of the integrable AL persist even in the saturable model.

We conclude by mentioning that the Peregrine-like waveforms portrayed in Fig. 8 are prone to modulational instability (MI). However, the MI effects are enhanced after their formation and not shown herein.

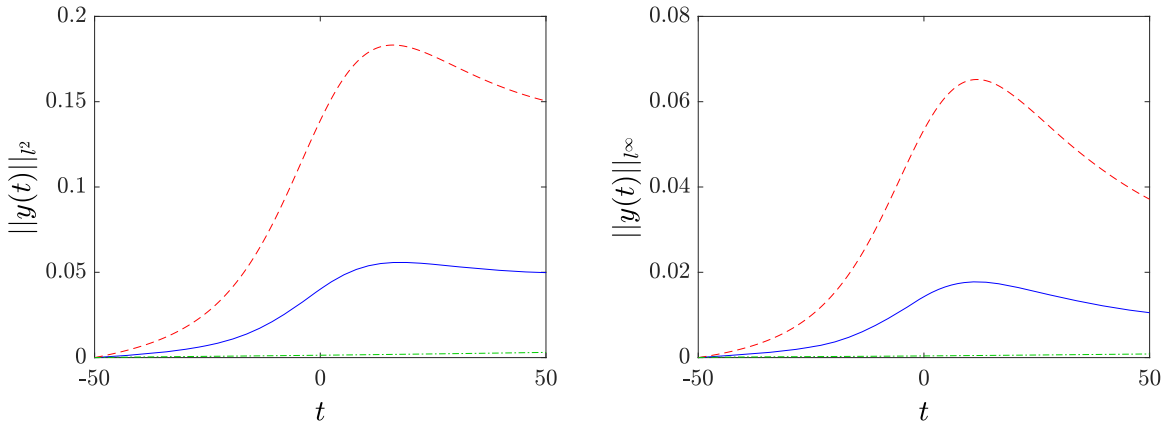

FIG. 9. Time evolution of $\|y(t)\|_{l^2}$ (left panel) and $\|y(t)\|_{l^\infty}$ (right panel), corresponding to the Peregrine soliton dynamics shown in Fig. 8 for the saturable DNLS (red dashed curve), the quintic G-AL (1.6) (green dashed-dotted curve), and the cubic DNLS (blue continuous curve).

V. CONCLUSIONS

In this work, we have continued our analytical and numerical investigations of the closeness of solutions between the integrable Ablowitz–Ladik lattice and non-integrable lattices for which the discrete nonlinear Schrödinger equation serves as the basic underlying model. With our analytical studies, we have established the closeness of solutions, in the sense of a continuous dependence on their initial data, between the Ablowitz–Ladik system and its important generalization with an extended power-law nonlinearity. The numerical investigations have further explored the issue of closeness of solutions for the generalized Ablowitz–Ladik system and the discrete nonlinear Schrödinger equation with a power-law nonlinearity and with saturable nonlinearity. For all these examples of non-integrable systems, the numerical studies justified, in full accordance with analytical predictions, that small amplitude solitonic structures possessing the form of the analytical solutions of the Ablowitz–Ladik system can be excited in nonintegrable lattices and survive for significantly long time intervals. One of the most striking examples is the persistence of spatiotemporal waveforms close to the analytical discrete Peregrine soliton, in all of the above-mentioned non-integrable lattices.

Future considerations may consider other DNLS systems important for physical applications (such as those relevant for the dynamics of granular crystals[27]), lattices incorporating gain and loss effects,[28] and crucially, extensions of our closeness approach to second-order in time lattice dynamical systems (as an example, we mention the closeness between the integrable Toda lattice[29] and Fermi–Pasta–Ulam–Tsingou lattices[30,31] or discrete Klein–Gordon systems[32]). Such investigations are in progress, and the results will be reported elsewhere.

ACKNOWLEDGMENTS

The authors would like to thank the referee for constructive comments and suggestions. J.C.-M. acknowledges support from EU (FEDER program 2014-2020) through both Consejería de Economía, Conocimiento, Empresas y Universidad de la Junta de Andalucía (under Project Nos. P18-RT-3480 and US-1380977), and MICINN and AEI (under Project Nos. PID2019-110430GB-C21 and PID2020-112620GB-I00.

AUTHOR DECLARATIONS

Conflict of Interest

The authors have no conflicts to disclose.

DATA AVAILABILITY

The data that support the findings of this study are available within the article.

REFERENCES

[1] M. J. Ablowitz and J. F. Ladik, "Nonlinear differential-difference equations and Fourier analysis," J. Math. Phys. **17**, 1011–1018 (1976).
[2] M. J. Ablowitz and J. F. Ladik, "A nonlinear difference scheme and inverse scattering," Stud. Appl. Math. **55**, 213–229 (1976).
[3] B. M. Herbst and M. J. Ablowitz, "Numerically induced chaos in the nonlinear Schrödinger equation," Phys. Rev. Lett. **62**, 2065 (1989).
[4] M. J. Ablowitz and P. A. Clarkson, *Solitons, Nonlinear Evolution Equations and Inverse Scattering* (Cambridge University Press, New York, 1991).
[5] L. D. Faddeev and L. A. Takhtajan, *Hamiltonian Methods in the Theory of Solitons* (Springer-Verlag, Berlin, 1987).
[6] V. E. Vekslerchik, "Functional representation of the Ablowitz–Ladik hierarchy," J. Phys. A: Math. Gen. **31**, 1087–1099 (1998).
[7] K.-i. Maruno and Y. Ohta, "Casorati determinant form of dark soliton solutions of the discrete nonlinear Schrödinger equation," J. Phys. Soc. Jpn. **75**, 054002 (2006).
[8] A. Ankiewicz, N. Akhmediev, and J. M. Soto-Crespo, "Discrete rogue waves of the Ablowitz-Ladik and Hirota equations," Phys. Rev. E **82**, 026602 (2010).
[9] N. Akhmediev and A. Ankiewicz, "Modulation instability, Fermi-Pasta-Ulam recurrence, rogue waves, nonlinear phase shift, and exact solutions of the Ablowitz-Ladik equation," Phys. Rev. E **83**, 046603 (2011).
[10] D. Hennig, N. I. Karachalios, and J. Cuevas-Maraver, "The closeness of the Ablowitz-Ladik lattice to the discrete nonlinear Schrödinger equation," J. Differ. Equations **316**, 346–363 (2022).
[11] J. Cuevas-Maraver, P. G. Kevrekidis, B. A. Malomed, and L. Guo, "Solitary waves in the Ablowitz–Ladik equation with power-law nonlinearity," J. Phys. A: Math. Theor. **52**, 065202 (2019).
[12] E. W. Laedke, K. H. Spatschek, and S. K. Turitsyn, "Stability of discrete solitons and quasicollapse to inrinsically lcalized modes," Phys. Rev. Lett. **73**, 1055–1059 (1994).
[13] O. Bang, J. J. Rasmussen, and P. L. Christiansen, "Subcritical localization in the discrete nonlinear Schrödinger equation with arbitrary power nonlinearity," Nonlinearity **7**, 205–218 (1994).
[14] P. Pacciani, V. V. Konotop, and G. Perla Menzala, "On localised solutions of discrete nonlinear Schrödinger equation: An exact result," Physica D **204**, 122–133 (2005).
[15] P. L. Christiansen, Yu. B. Gaididei, V. K. Mezentsev, S. L. Musher, K. Ø. Rasmussen, J. J. Rasmussen, I. V. Ryzhenkova, and S. K. Turitsyn, "Discrete localized states and localization dynamics in discrete nonlinear Schrödinger equations," Phys. Scr. **1996**(T67), 160–166.
[16] J. Cuevas and J. C. Eilbeck, "Discrete soliton collisions in a waveguide array with saturable nonlinearity," Phys. Lett. A **358**, 15–20 (2006).
[17] L. Hadzievski, A. Maluckov, M. Stepić, and D. Kip, "Power controlled solitons stability and steering in lattices with saturable nonlinearity," Phys. Rev. Lett. **93**, 033901 (2004).
[18] M. Stepic, D. Kip, L. Hadzievski, and A. Maluckov, "One-dimensional bright discrete solitons in media with saturable nonlinearity," Phys. Rev. E **69**, 066618 (2004).
[19] R. A. Vicencio and MM. Johansson, "Discrete soliton mobility in two dimensional waveguide arrays with saturable nonlinearity," Phys. Rev. E **73**, 046602 (2006).
[20] T. R. O. Melvin, A. R. Champneys, P. G. Kevrekidis, and J. Cuevas, "Radiationless travelling waves in saturable nonlinear Schrödinger lattices," Phys. Rev. Lett. **97**, 124101 (2006).

[21] J. Wu, "The inviscid limit of the complex Ginzburg–Landau equation," J. Differ. Equations **142**, 413–433 (1998).
[22] T. Ogawa and T. Yokota, "Uniqueness and inviscid limits of solutions for the complex Ginzburg-Landau equation in a two-dimensional domain," Commun. Math. Phys. **245**, 105–121 (2004).
[23] M. H. Hays, C. D. Levermore, and P. D. Miller, "Macroscopic lattice dynamics," Physica D **79**, 1–15 (1994).
[24] O. Dutta, M. Gajda, P. Hauke, M. Lewenstein, D.-S. Lühmann, B. A. Malomed, T. Sowiński, and J. Zakrzewski, Non-standard Hubbard models in optical lattices: A review, Rep. Prog. Phys. **78**, 066001 (2015).
[25] M. Salerno, "Quantum deformations of the discrete nonlinear Schrödinger equation," Phys. Rev. A **46**, 6856–6859 (1992).
[26] D. Cai, A. R. Bishop, and N. Grønbech-Jensen, "Localized states in discrete nonlinear Schrödinger equation," Phys. Rev. Lett. **72**, 591–595 (1994).
[27] G. James, "Travelling breathers and solitary waves in strongly nonlinear lattices," Philos. Trans. R. Soc. London, Ser. A **376**, 20170138 (2018).
[28] Y. V. Kartashov, B. A. Malomed, and L. Torner, "Solitons in nonlinear lattices," Rev. Mod. Phys. **83**, 247–305 (2011).
[29] M. Toda, *Theory of Nonlinear Lattices* (Springer-Verlag, Berlin, Heidelberg, 1989).
[30] Y. V. Lvov and M. Onorato, "Double scaling in the relaxation time in the β-Fermi-Pasta-Ulam-Tsingou model," Phys. Rev. Lett. **120**, 144301 (2018).
[31] G. P. Berman and F. M. Izrailev, "The Fermi–Pasta–Ulam problem: Fifty years of progress," Chaos **15**, 015104 (2005).
[32] S. Flach and A. V. Gorbach, "Discrete breathers—Advances in theory and applications," Phys. Rep. **467**, 1–116 (2008).